

# A field study on distributed fiber optic deformation monitoring of overlying strata during coal mining

Gang Cheng<sup>1</sup> · Bin Shi<sup>1</sup> · Hong-Hu Zhu<sup>1</sup> · Cheng-Cheng Zhang<sup>1</sup> · Jing-Hong Wu<sup>1</sup>

Received: 15 January 2015/Revised: 25 July 2015/Accepted: 30 July 2015/Published online: 18 September 2015  
© Springer-Verlag Berlin Heidelberg 2015

**Abstract** In this paper, the distributed optical fiber sensing technology based on Brillouin optical time-domain reflectometer (BOTDR) was employed to monitor and analyze the force and deformation of the overlying rock strata during the coal mining process in Huaibei, China. The selection and arrangement of the sensing cables were introduced, together with details on data collection and analysis. Four types of sensing cables were vertically installed into a borehole to monitor the strata deformation. The monitoring data were collected according to the mining schedule. The strain distributions and their variations with time were studied to reveal the deformation pattern of the overlying rock mass induced by coal mining. Results showed that during the mining process, there was a fracture surface at the bottom of the upper igneous rock layer. The separation phenomenon occurred along the fracture surface in the lower rock strata, which slipped obliquely to coal-face. The rock beneath the bottom of the lower igneous rock layer was compressed due to periodic weighting of the overlying rock strata before the working face reached the monitoring borehole. The ground deformation gradually accumulated during the whole mining process. These results indicate that the BOTDR-based monitoring method is effective for capturing strata deformation induced by underground mining, and may open up new avenues for ensuring safe and efficient coal mining activities.

**Keywords** Distributed optical fiber sensing · Coal mining · Overlying strata · Brillouin optical time-domain reflectometer (BOTDR)

## 1 Introduction

The deformation of overlying rock mass during underground mining has been one of the most critical problems that affect the safety and efficiency of coal mining activities [1]. Deformation prediction of overlying strata during the mining process is of great importance for preventing water-related mine disasters. With the development of modern monitoring technologies, a variety of methods have been proposed to study the deformation and failure of overlying strata. Currently, the commonly used methods are empirical modeling [2, 3], geomechanical model testing [4], numerical simulation [5], and electromagnetic exploration [6]. The utilization of these methods effectively improves the estimation of overlying rock deformation and provides valuable information for ensuring the safety and efficiency of coal mining. However, the above methods suffer from low level of quantification for practical applications. It is, therefore, difficult to capture the whole process of deformation and potential failure of the overlying strata during mining activities.

In the recent years, optical fiber sensing technologies have developed rapidly and are being recognized as a promising monitoring method [7–10]. The Brillouin optical time-domain reflectometer (BOTDR)-based optical fiber strain sensor has emerged with a variety of advantages, such as distributed and long-distance measurement, corrosion resistance, and anti-electromagnetic interference. These sensors have been used for strain monitoring and

✉ Bin Shi  
shibin@nju.edu.cn

Hong-Hu Zhu  
zhz@nju.edu.cn

<sup>1</sup> School of Earth Sciences and Engineering, Nanjing University, Nanjing 210046, China

health diagnosis of slopes, underground structures, pipelines, bridges, and other major infrastructures [11–18].

A mine site in Huaibei, China is invaded by large areas of magmatic rock. The coal layer is covered by many layers of igneous rock, resulting in unique mining conditions and serious engineering geological problems. In order to study the influence of coal mining on the deformation of overlying rock strata, field instrumentation with high degree of accuracy should be used.

In this paper, a BOTDR-based distributed measurement method was proposed to monitor the deformation of overlying strata in this mining project. The rock deformations and their variations during the whole process of mining were studied. These results demonstrate that the distributed optical fiber sensing technology is of great potential for deformation monitoring during underground mining.

## 2 Working principle of BOTDR

BOTDR monitoring technology is based on the spontaneous Brillouin scattering (SBS) light in fiber, which can measure the change of temperature and strain along the whole distributed sensing [19]. The frequency of Brillouin scattered light will generate drift with respect to the frequency of injection pulse light [20, 21]. The frequency shift has a linear relationship with axial strain or temperature changes which the fiber suffers [22], as shown in Fig. 1.

Strain and temperature measurements of a host material are realized by BOTDR using the following relationship:

$$v_B(\varepsilon, T) = v_B(0, T_0) + \frac{\partial v_B(\varepsilon)}{\partial \varepsilon} \cdot \varepsilon + \frac{\partial v_B(T)}{\partial T} \cdot (T - T_0) \quad (1)$$

where  $\varepsilon$  is strain;  $T$  is temperature;  $v_B(\varepsilon, T)$  is Brillouin frequency shift (BFS) with strain and temperature;  $v_B(0, T_0)$  is BFS at the initial temperature  $T_0$  without strain;  $\partial v_B(\varepsilon)/\partial \varepsilon$  and  $\partial v_B(T)/\partial T$  are the strain and temperature coefficients, respectively;  $\partial v_B(T)/\partial T$  is the proportional coefficient of temperature which is about 1.43 MHz ( $^{\circ}\text{C}$ ) at the wavelength  $\lambda = 1.55 \mu\text{m}$ ;  $(T - T_0)$  is the temperature change of the optical fiber.

Under a constant temperature, the above equation can be expressed as

$$v_B(\varepsilon) = v_B(0) + \frac{dv_B(\varepsilon)}{d\varepsilon} \varepsilon \quad (2)$$

where  $\varepsilon$  is strain;  $v_B(\varepsilon)$  is BFS with strain;  $v_B(0)$  is BFS without strain; and  $dv_B(\varepsilon)/d\varepsilon$  is the proportional coefficient of strain which is about 493 MHz ( $\%$  strain) at the wavelength  $\lambda = 1.55 \mu\text{m}$ .

When a pulsed light is launched at one end of an optical fiber, the BOTDR instrument launches the pulsed light and

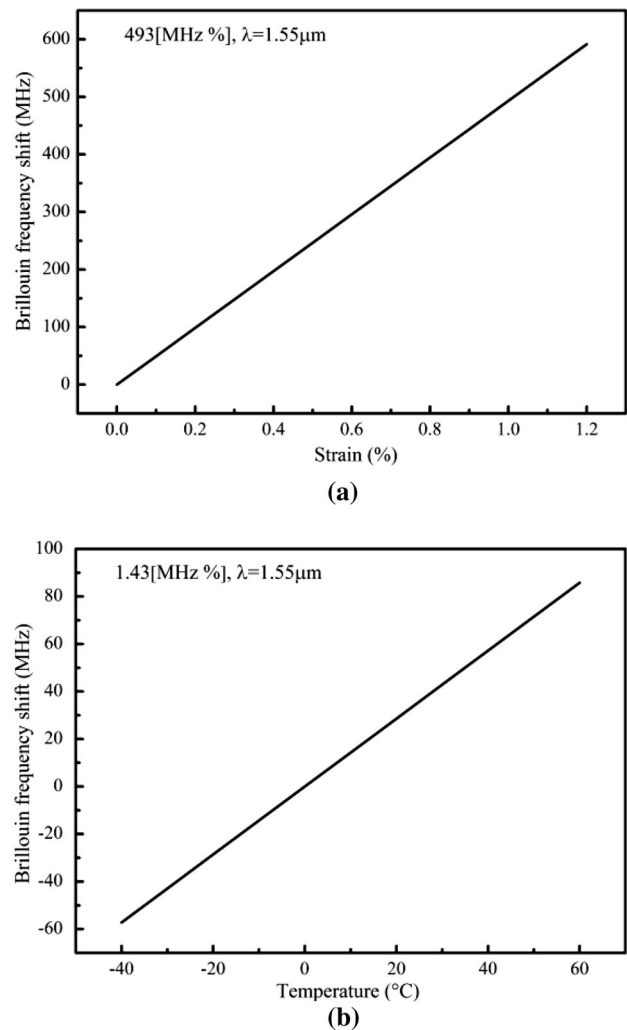


**Fig. 1** Relationship between Brillouin frequency shift and **a** strain and **b** temperature

receives the Brillouin backscattered light at the same end (see Fig. 2a). The traveled distance from the position where pulsed light is launched to the position where the scattered light is generated can be determined using the following equation:

$$X = cT/2n \quad (3)$$

where  $c$  is the velocity of light in a vacuum,  $T$  is the time interval between the launching of the pulse light and the receiving of the scattered light at the end of the optical fiber, and  $n$  is the refractive index of the optical fiber.

When a certain part of optical fiber is strained, its BFS  $v_B$  will become  $v_B'$ , which results in the rapid decrease of the Brillouin scattering signal (see Fig. 2b). By slightly changing the frequency of the incident light, the Brillouin scattering signal of this strained part can be received again (see Fig. 2c). In this way, the BFS at each point along the optical fiber can be measured.

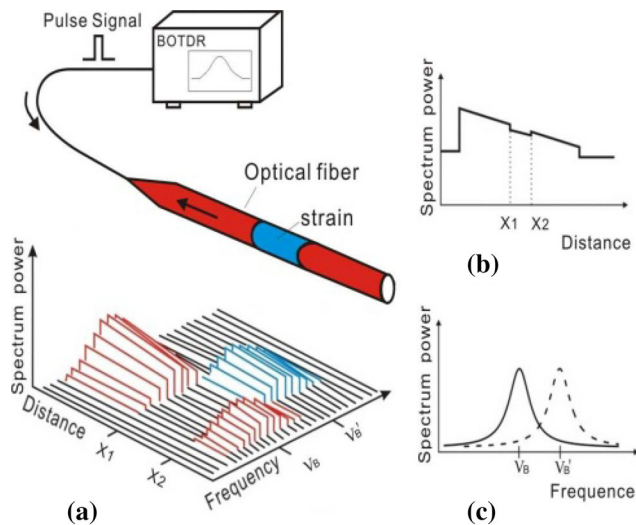


**Fig. 2** Configuration of BOTDR [23]

### 3 Profiles of strata

To investigate the potential of BOTDR in monitoring rock strata deformation during mining, a field trial was conducted. The mine site is located in the northern part of the alluvial plain of Huaibei, and the terrain is very flat within the mine field. In addition to ditches, villages, and paths, the rest of the terrain is covered by farmland. The strata are mainly Cenozoic loose layers with the thicknesses ranging between 121.00 and 196.50 m. The main working bed is No. 10 coal seam with an average thickness of 3.11 m, which is the key monitoring coal seam in this project.

The overlying rock strata of the coal seam are composed of Quaternary and Tertiary sediments, mudstone and sandstone. In addition, there are two layers of igneous rock, the thicknesses of which are 28.55 and 48.30 m, respectively. Details on the geological conditions of this mine site are shown in Fig. 3.

### 4 Monitoring program

#### 4.1 Selection of the sensing cables

Four types of fiber optic sensing cables were selected in the monitoring project. They have different sensing functions and performances in terms of optical properties, mechanical strength, and strain transfer efficiency. All the cables can meet the requirement of large deformation measurement and have high strength and excellent sensing performance. To monitor the deformation of the rock strata with a total depth of 600 m, the four sensing cables with three different intervals and different monitoring ranges were installed in the field. Details of these sensing cables

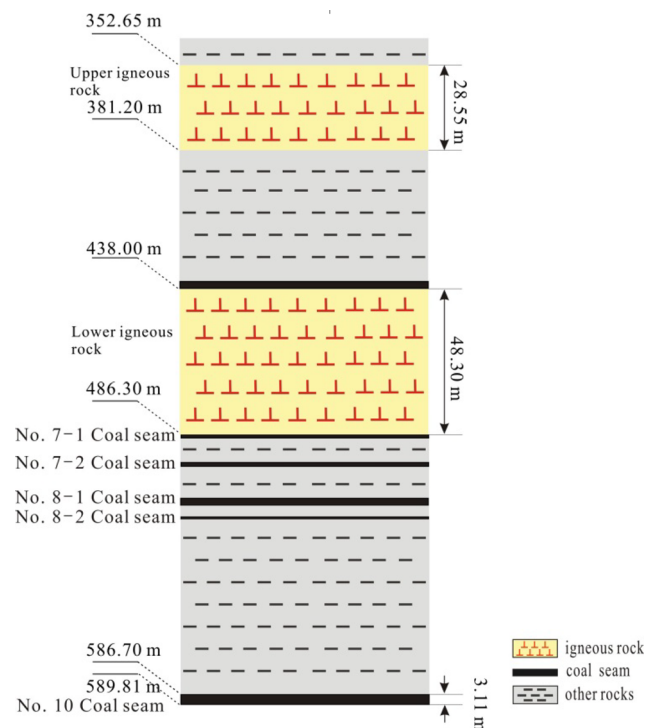


**Fig. 3** Stratigraphic column of the study area

are listed in Table 1, and the cross-sectional structures are shown in Fig. 4.

#### 4.2 Test equipment

A BOTDR-based N8511 optical fiber strain analyzer fabricated by Advantest Co. Ltd. in Japan was used for data collection in this study. The main technical parameters of the BOTDR analyzer are shown in Table 2. Because there was no power supply at this project site and the transportation of the BOTDR analyzer was very inconvenient, a remote long-term monitoring scheme was adopted. A 3.7-km-long optical cable was laid out from the borehole to a monitoring station for remote data collection.

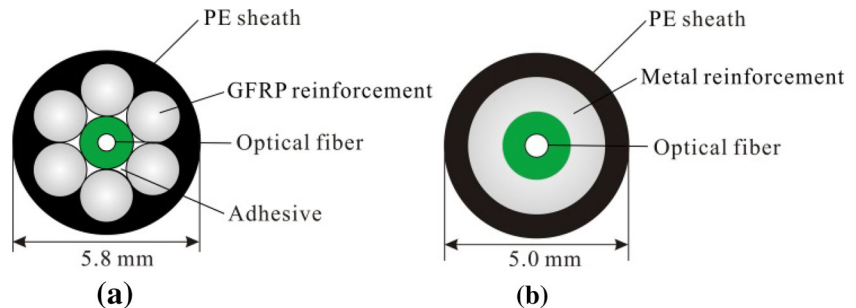
#### 4.3 Monitoring scheme

The main purpose of this monitoring project is to investigate the deformation of the overlying rock strata during the whole process of coal mining, and the strata separation in particular. According to the monitoring project, a monitoring borehole with an internal diameter of 91 mm and a depth of 600 m was drilled perpendicular to the No. 10 coal seam, as shown in Fig. 5.

Four fiber optic sensing cables were installed in the monitoring borehole: GFRP optical cable, 20-m-interval fixed-point optical cable, 50-m-interval fixed-point optical cable, and strata fixed-point optical cable. To facilitate the

**Table 1** Details of the four sensing cables selected in the monitoring project

Cable type	Outer diameter (mm)	Tensile strength (N)	Strain range (%)	Feature	Monitoring range (m)
GFRP cable	5.8	4500	−1 to 1	Small deformation monitoring	0–595
Fixed-point cable (20-m interval)	5.0	3000	0–5	Continuous large deformation monitoring	175–595
Fixed-point cable (50-m interval)					308–595
Fixed-point cable (fixed at five strata)					274–595

**Fig. 4** Cross-sectional view of the sensing cables. **a** GFRP cable, and **b** Fixed-point cable**Table 2** Specifications of the N8511 strain analyzer

Measurement range (km)	1, 2, 5, 10, 20, 40, 80				
Spatial sampling interval (m)	0.05, 0.10, 0.20, 0.50, 1.00				
Pulse width (ns)	10	20	50	100	200
Dynamic range (dB)	3.5	7.5	11.5	14.5	16.5
Strain measurement repeatability	$< \pm 100 \mu\epsilon$				
Strain measurement range	$-1.5 \% \sim 1.5 \% (15000 \mu\epsilon)$				
Sampling frequency range (GHz)	10~12				
Measurement frequency step (MHz)	1, 2, 5, 10, 20, 50				
Spatial positioning accuracy (m)	$\pm(5.0 \times 10^{-5} \times \text{Measurement range (m)} + 0.2 \text{ m} + 2 \times \text{Distance sampling interval (m)})$				

installation of the sensing cables in the borehole, a drill bar with a guiding cone was utilized. The heads of the cables were fixed to the cone and then inserted in the borehole. Then, the borehole was grouted, and the drill bar was removed. Detailed installation procedures of the cables are as follows.

- (1) The sensing cables were divided into two groups and were fixed onto the guiding cone using epoxy resin.
- (2) Before the cables were inserted into the borehole, the hole was cleaned carefully.
- (3) The guiding cone was further fixed to a 50-mm-diameter drill bar and was then inserted into the borehole. Care was taken during this procedure.
- (4) Once the drill bar reached the bottom of the hole, the guiding cone was separated from the drill bar under the self-weight of the cone ( $m = 15 \text{ kg}$ ).
- (5) Then, the hole was grouted using a mixture of cement, silt, and fly ash. Several trials were conducted to determine the optimum ratio of the mixture.
- (6) Finally, the hole was sealed, and the free segments of the sensing cables were protected carefully. The lengths of the effective segment of the sensing cables were 595 m.

#### 4.4 Data collection

The initial measurements were obtained after the cement grout was cured (July 10, 2013). The data were used as zero reference points. Afterward, the strains were measured continually according to the mining progress until December 25, 2013. During the mining process, the open-

**Fig. 5** Schematic illustration of the sensing cables layout in the monitoring borehole

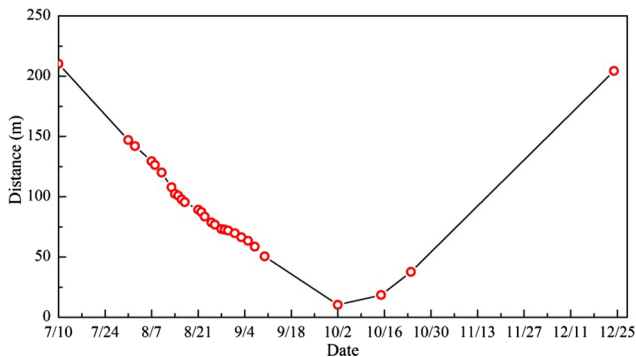
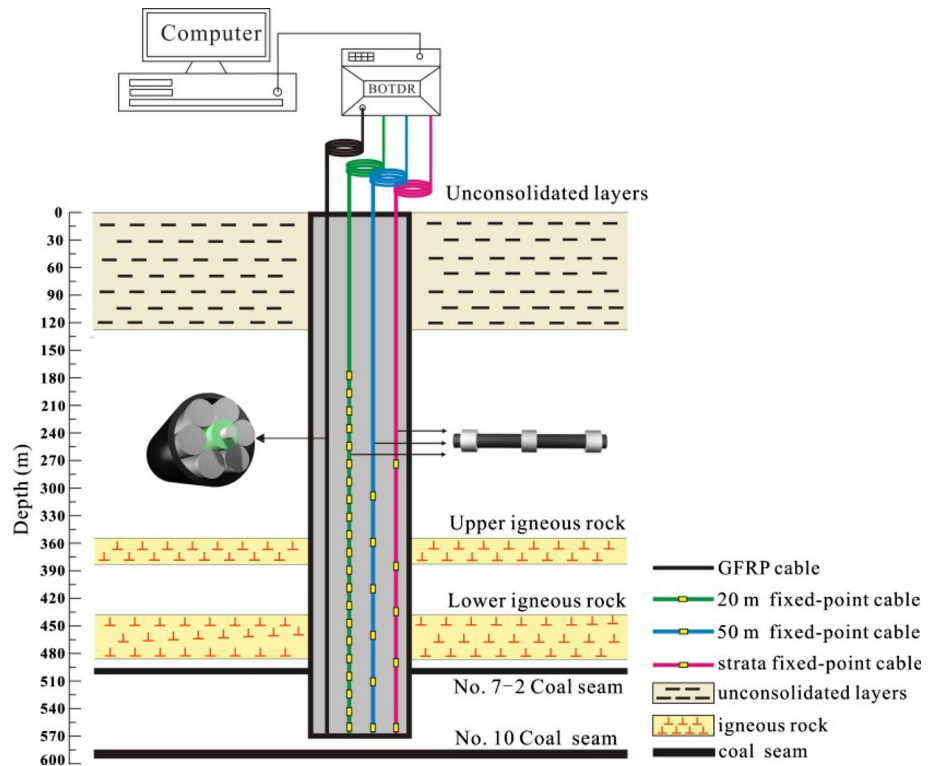


**Fig. 6** Variation of horizontal distance between the open-off cut and the borehole with the process of mining

off cut first got close to the borehole and then moved away, as shown in Fig. 6. Because the temperature variations in the deep rock were quite small and the influence of rock deformation on the monitoring data was much larger than the temperature effect, temperature compensation of the strain measurements was not conducted in this project.

## 5 Monitoring results and analysis

### 5.1 Deformation of overlying strata

During the mining process, the sensing cables got damaged one by one due to the large strata deformation. Details on

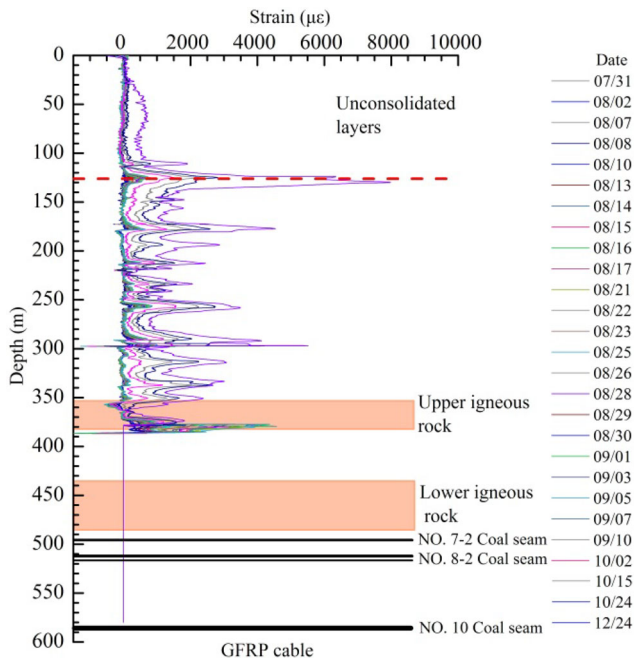
the breakages of the sensing cables are shown in Table 3. The GFRP cable was broken on July 31. This indicates that the overlying rock layers had been significantly influenced by the mining activity that occurred far away from the monitoring borehole ( $s = 147.1$  m).

The strain monitoring results of four cables are shown in Figs. 7, 8, 9, and 10. In these figures, a positive strain represents tensile deformation of the rock, while for compression, the strain is negative. The rock strata overlying the coal seam had tensile or compressive deformation during the process of coal mining. The compressive stress on the rock above coal seam was induced by periodic weighting, which resulted from the mining activity before the working face reached the monitoring borehole.

Figures 7, 8, 9, and 10 show that, downward rock movements above the upper igneous rock layer occurred and accumulated during mining. The upper igneous rock layer should be the key stratum according to the key strata theory [24]. In the initial mining stage of working face and before the key stratum is broken, the overlying strata gradually settled down in the deformation form of a beam or a plate on elastic foundation. According to the key strata theory, since the mining was super deep, a significant strata separation would occur under the key stratum, i.e., the upper igneous rock layer. The monitoring results clearly demonstrate this phenomenon. Before the working face passed through the monitoring borehole, there were small strains in the four sensing cables above the bottom of the

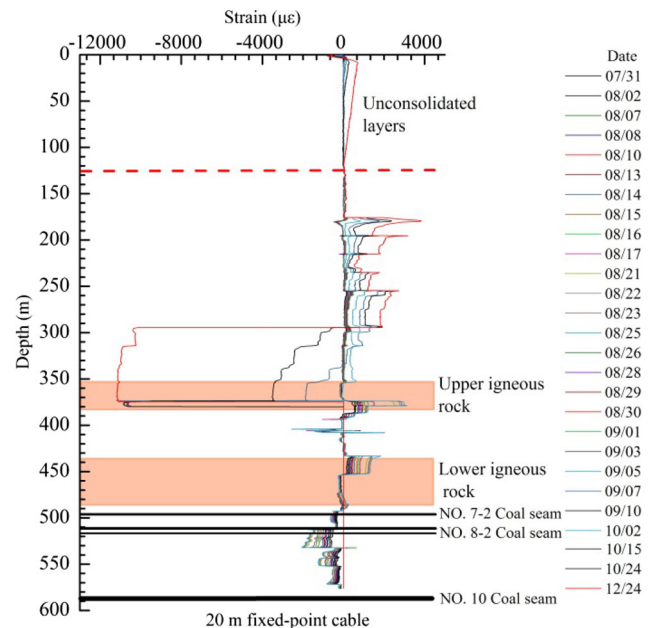
**Table 3** Situation of fiber optic breakages and mining line

Cable type	Broken date	Horizontal distance between open-off cut and borehole (m)	Initial horizontal distance (m)
GFRP cable	07/31	147.1	192.6
Fixed-point cable (20-m interval)	08/30	71.9	
Fixed-point cable (50-m interval)	08/24	81.4	
Fixed-point cable (fixed at five strata)	08/27	74.9	

**Fig. 7** Monitoring results of the GFRP cable

upper igneous rock layer, which illustrated that these strata were relatively stable. However, tensile strains rapidly accumulated at the bottom of the upper igneous rock layer. There was an apparently critical zone around the depth of 390 m, where strata separations and fissures developed. With the continuous advances of the working face, strata separation became more obvious, and finally all the four sensing cables become broken at this location. The above observations are consistent with the key strata theory, which in turn verified the effectiveness of the fiber optic technology in mining monitoring.

As shown in Figs. 8, 9, and 10, while the working face passed through the monitoring borehole, the compressive strain of the sensing fiber increased gradually at the drilling depth of 450–580 m. It indicates that the advanced support pressure of the overlying strata increased gradually as well. The strains of the three sensing cables were relatively large at the depth of 490 m, indicating that the strata behaviors induced by mining distributed between the fault zone and the depth of 490 m.

**Fig. 8** Monitoring results of the 20-m-interval fixed-point cable

Figures 7, 8, 9, and 10 show that, during the period from July 10 to August 30, the rock strata beneath the bottom of the lower igneous rock layer were compressed by periodic weighting of the overlying rock, and the deformation increased gradually during the mining process. Because the sensing cables have been broken, the strata deformation below the damage points could not be measured anymore. In addition, the lower rock ( $s = 480\text{--}580\text{ m}$ ) of No. 7-2 coal seam was in the compression state due to the periodic weighting of the overlying strata. The deformation of the cables can be express by Eq. (4):

$$\Delta L = \int_{z_1}^{z_2} \varepsilon(z) dz \quad (4)$$

where  $\Delta L$  is the deformation between  $z_1$  and  $z_2$ ,  $z_1$ ,  $z_2$  are the points on the cables; and  $\varepsilon(z)$  are the strain values of cable at point  $z$ . Up to August 30, the total deformation of the compression zone is calculated to be about 76 mm. The strata between the two igneous rock layers were in a tensioned state with a total deformation of about 27 mm. It is

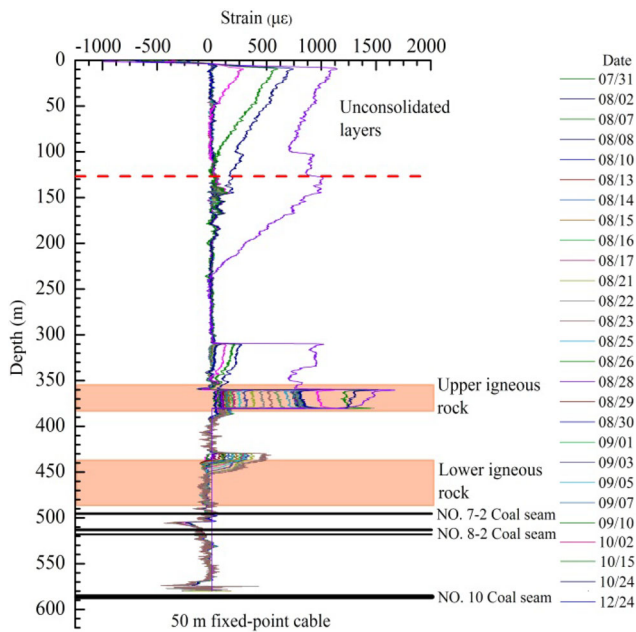


**Fig. 9** Monitoring results of the 50-m-interval fixed-point cable

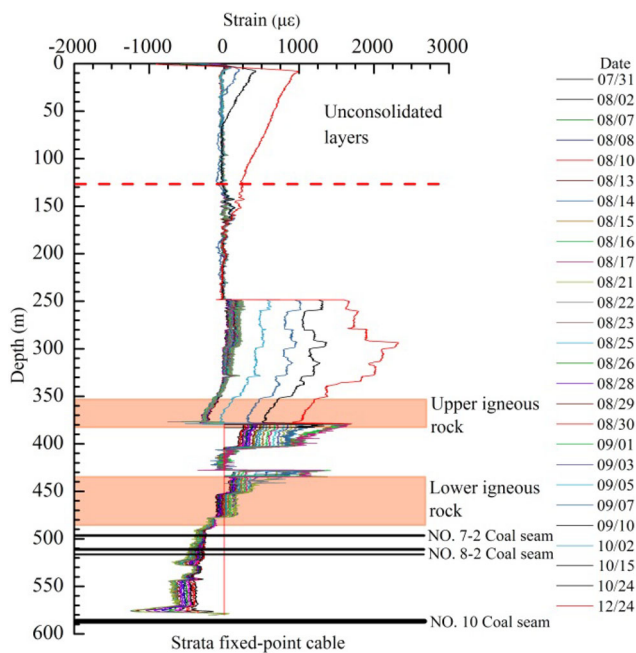


**Fig. 10** Monitoring results of the strata fixed-point cable

also shown that the lower igneous rock was in a tensioned state, and the deformation was about 27 mm.

**5.2 Comparison of different cables**

Different types of sensing cables show different strain distributions during the mining process. As shown in Fig. 7, the data measured by tight-buffed GFRP cables

show evident fluctuations and peaks. These values reflect the small deformation of rock mass. In addition, the captured data facilitate the separation of the deformations from strata and those between adjacent strata. Therefore, these data can reflect the amount and the distribution of the external loads, and capture the evolutions before an abscission occurs. Once an abscission forms, a large amount of microstrains occur. If local strains exceed the ultimate measurement range of the sensing cable, the cable will break. From Figs. 8, 9, and 10, it is seen that fixed-point cables widens the measurement ranges by averaging the deformation of rock mass to each fixed-point section, which realizes the monitoring of large continuous deformations of strata. Contrary to tight-buffed GFRP cables, the monitoring data from fixed-point cables are smoother. An evident advantage of these cables is that the data can reflect the deformations of strata at different depths. With the help of these cables, one can calculate the accurate deformation of a certain stratum. According to the results shown in Figs. 8, 9, and 10, one can tell that the strains from the 20-m-interval fixed-point cable are the largest.

**5.3 Deformation characteristics of abscission layer**

After the working face passed the borehole, the stress state of the overlying rock changed from compressive stress to tensile stress due to the missing of support from the overlying rock. In addition, fractures and abscissions formed as well at that time. With the advancing of the working face, the overlying rock deformed continuously, and stress concentration occurred at the depth of 390 m with a maximum recorded strain of 1650 µε (Fig. 9). These phenomena lead to the conclusion that there is a fracture surface between the bottom of the upper igneous rocks and lower part of the rock; the separation phenomenon occurs along the fracture surface in the lower part of the rock.

Figure 11 shows the strain variation of the abscission layer at the depth of 390 m with the advancing of the working face. It is observed that the strains increased linearly with the advancing of the working face before the borehole was reached. After the working face passed the borehole, the variation of the strain was consistent with those observed from common overlying rocks barring minor differences.

According to the monitoring schedule and data, the variation of the maximum testing depth of four cables with the mining progress (time and distance) can be obtained. The changes of monitoring cables with the coal mining can be clearly seen from Figs. 12 to 13. It provides a reliable basis for analyzing large deformation and separation location, and also provides reference for the improvement and selection of monitoring cables for deep borehole monitoring in the future.

### 5.4 Height determination of caving zone and fractured zone

During the mining process, the deformation behavior of the overlying strata can be divided into three categories, i.e., large rock deformation, large interlayer deformation (an indicator of strata separation), small rock deformation. According to the monitoring results of the distributed fiber optic sensing cables, the deformation pattern of the overlying strata can be easily determined. In this case study, although some monitoring data were lost due to cable damage, the remaining results indicate that large interlayer deformation occurred at the bottom of the upper igneous

rock layer and at the top of the lower igneous rock layer. The upper igneous rock layer had much smaller internal deformation than the lower layer.

According to the strain distribution characteristics of the cables, the heights of the fractured and caving zones can be inferred. As shown in Figs. 9, and 10, there were two stress concentration areas at the depths of 574 and 530 m. Therefore, the heights of the caving and fractured zones were estimated to be around 12.7 and 56.7 m, respectively. According to the Mining Specification of China [25], if the mining thickness was 3 m, the height of the caving zone was  $13.4 \pm 2.5$  m, and the height of the fractured zone was  $53.6 \pm 5.6$  m. The calculation results fit well with the field observations.

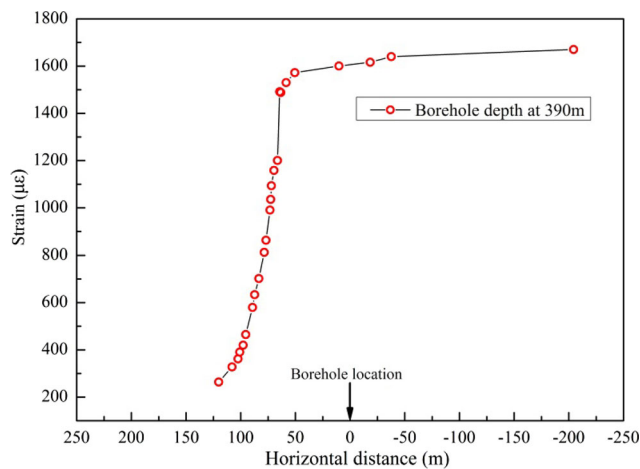
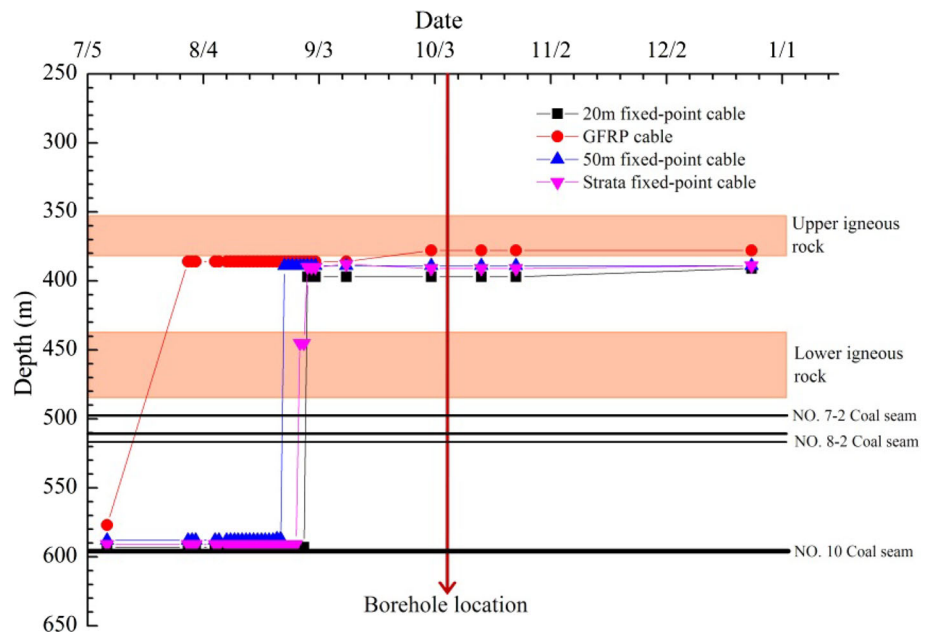


**Fig. 11** Strain variations of abscission layer at the depth of 390 m with the advancing of the working face

**Fig. 12** Variation of the maximum testing depths of four cables with the mining progress (time)



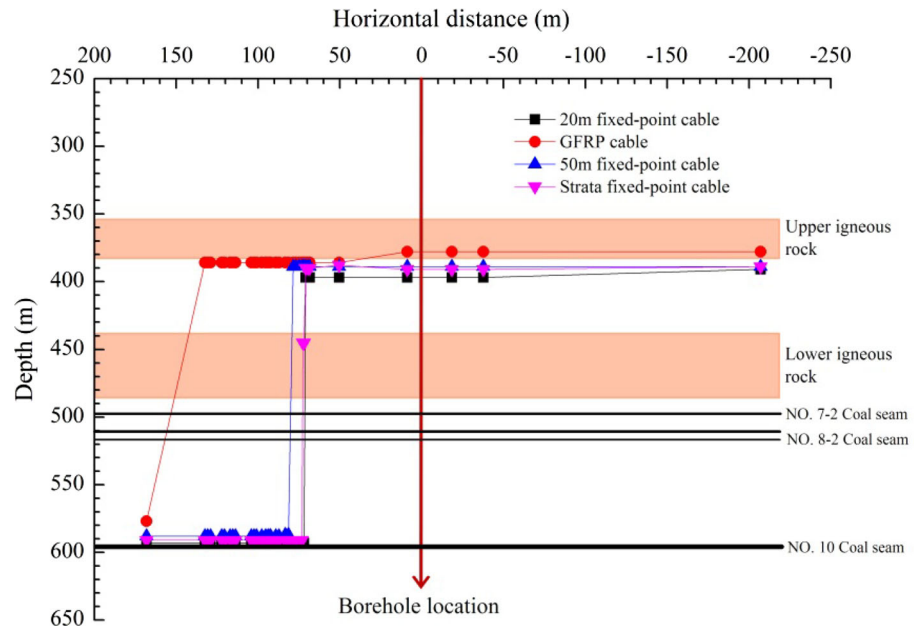
### 6 Conclusions

In this study, the deformation of overlying rock strata in a mine site was monitored using distributed optical fiber sensing technology. Based on the above analyses, the following conclusions are obtained:

- (1) During the process of coal mining, the deformation of the overlying rock mass can be monitored using distributed fiber optic monitoring technology, and the stress state of the overlying rock can be obtained in real time by using this method.
- (2) With the mining of No. 10 coal seam, when the open-off cut is away from the monitoring borehole, the strain of the rock at the top of the coal seam (drilling depth was 450–580 m) decreases gradually



**Fig. 13** Variation of the maximum testing depths of four cables with the mining progress (distance)



due to periodic weighting of the overlying rock. The strain of this part of rock decreases gradually; therefore, a compression state is presented. The compression effect decreases gradually due to periodic weighting of this part of rock mass and the rocks finally tension; the amount of tensile deformation is increasing. According to the actual strata, it is indicated that the lower igneous rock is the boundary mark of different stress states. The rock above the lower igneous rock shows tensile deformation due to its self-weight; the rock below the lower igneous rock first gets compressed and then suffers tension, and the stress state of the lower rock changes continuously during the whole process.

- (3) From the measured strain data of the whole monitoring periods, it is found that the four cables are broken at the bottom of the upper igneous rock. The lower part of the igneous rock is greatly affected by coal mining, and some relatively large separations occur; the lower igneous rock and its surrounding rock are broken. There are some separations occurring in the upper igneous rocks and the overlying rock mass; however, the rock mass is relatively intact. A relatively large separation is formed in the bottom of the upper igneous rock, which may result in the accumulation of much water and mash gas during the process of mining. Therefore, it is important to pay attention to the treatment of the gathered water and mash gas in the separation during the mining process.

**Acknowledgments** This study is financially supported by the National Natural Science Foundation of China (Grant Nos. 41230636, 41372265, and 41427801).

## References

1. Palchik V (2005) Localization of mining-induced horizontal fractures along rock layer interfaces in overburden: field measurements and prediction. *Environ Geol* 48:68–80
2. Palchik V (2002) Influence of physical characteristics of weak rock mass on height of caved zone over abandoned subsurface coal mines. *Environ Geol* 42(1):92–101
3. Society for Mining, Metallurgy & Exploration, Inc (2013) *Modern American coal mining: methods and applications*. Society for Mining, Metallurgy & Exploration, Inc, Colorado
4. Zhang YJ, Li FM (2011) Monitoring analysis of fissure development evolution and height of overburden failure of high tension fully mechanized caving mining. *Chin J Rock Mech Eng* 30(S1):2994–3001 (in Chinese)
5. Gao F, Stead D, Coggan J (2014) Evaluation of coal longwall caving characteristics using an innovative UDEC Trigon approach. *Comput Geotech* 55:448–460
6. Zhang PS, Hu XW, Wu RX (2012) Study of detection system of distortion and collapsing of top rock by resistivity method in working face. *Rock Soil Mech* 3:952–956 (in Chinese)
7. Zhu HH, Shi B, Zhang J, Yan JF, Zhang J, Zhang CC, Wang BJ (2014) Fiber Bragg grating based performance monitoring of a model slope subjected to seepage. *Smart Mater Struct* 23(9):095027
8. Zhu HH, Shi B, Yan JF, Zhang J, Wang J (2014) Investigation of the evolutionary process of a reinforced model slope using a fiber-optic monitoring network. *Eng Geol* 186:34–43
9. Zhang CC, Zhu HH, Shi B, She JK (2014) Interfacial characterization of soil-embedded optical fiber for ground deformation measurement. *Smart Mater Struct* 23(9):095022

10. Zhang CC, Zhu HH, Shi B, Zhang D, She JK (2015) Quantitative evaluation of optical fiber/soil interfacial behavior and its implications for sensing fiber selection. *IEEE Sens J* 15(5):3059–3067
11. Lu Y, Shi B, Wei GQ, Chen SE, Zhang D (2012) Application of a distributed optical fiber sensing technique in monitoring the stress of precast piles. *Smart Mater Struct* 21:115011
12. Klar A, Dromy I, Linker R (2014) Monitoring tunneling induced ground displacements using distributed fiber-optic sensing. *Tunn Undergr Space Technol* 40:141–150
13. Piao CD, Shi B, Gao L (2011) Characteristics and application of BOTDR in distributed detection of pile foundation. *Adv Mater Res* 163–167:2657–2665
14. Zhu HH, Shi B, Zhang J, Yan JF, Zhang CC (2014) Distributed fiber optic monitoring and stability analysis of a model slope under surcharge loading. *J Mt Sci* 11(4):979–989
15. Mohamad H, Soga K, Pellew A, Bennett P (2011) Performance monitoring of a secant-piled wall using distributed fiber optic strain sensing. *J Geotech Geoenviron Eng* 137(12):1236–1243
16. Schwamb T, Soga K, Mair RJ, Elshafie MZEB, Sutherland R, Boquet C, Greenwood J (2014) Fibre optic monitoring of a deep circular excavation. *Geotech Eng* 167(2):144–154
17. Klar A, Bennett PJ, Soga K, Mair RJ, Tester P, Fernie R, John HDS, Torp-Peterson G (2006) Distributed strain measurement for pile foundations. *Geotech Eng* 159(3):135–144
18. Soga K (2014) Understanding the real performance of geotechnical structures using an innovative fibre optic distributed strain measurement technology. *Riv Ital Geotec* 4:7–48
19. Horiguchi T, Shimizu K, Kurashima T, Tateda M, Koyamada Y (1995) Development of a distributed sensing technique using Brillouin scattering. *J Lightwave Technol* 13:1296–1302
20. Wang BJ, Li K, Shi B, Wei GQ (2009) Test on application of distributed fiber optic sensing technique into soil slope monitoring. *Landslides* 6(1):61–68
21. Wu Z, Xu B, Takatada T, Harada T (2008) Performance of a BOTDR optical fiber sensing technique for crack detection in concrete structures. *Struct Infrastruct Eng* 4:311–323
22. Shi B, Xu HZ, Chen B, Zhang D, Ding Y, Cui HL, Gao JQ (2003) A feasibility study on the application of fiber-optic distributed sensors for strain measurement in the Taiwan Strait Tunnel project. *Mar Georesour Geotechnol* 21(3–4):493–499
23. Sun YJ, Shi B, Chen SE, Zhu HH, Zhang D, Lu Y (2014) Feasibility study on corrosion monitoring of a concrete column with central rebar using BOTDR. *Smart Struct Syst* 13(1):41–53
24. Miao XX, Chen RH, Pu H, Qian MG (2005) Analysis of breakage and collapse of thick key strata around coal face. *Chin J Rock Mech Eng* 24(8):1290–1296 (**in Chinese**)
25. State Bureau of Coal Industry (2000) Regulations of buildings, water, rail way and main well lane leaving coal pillar and press coal mining. China Coal Industry Publishing House, Beijing (**in Chinese**)